 SL, vol.6, no.3, pp.133-143, 2011

Numerical and Theoretical Studies of the Buckling of Shape Memory Tape Spring

Zhengfa Li[1], **Weibin Song and Zhengdao Wang**

Abstract: By using the high froze/recovery strains of shape memory polymers to meet the requirements of deployable space structures, the folding behavior of shape memory tape spring consisting of shape memory polymer and metal spring was analyzed. Firstly, numerical simulations were performed on the buckling modes and affecting factors under the equal- and opposite-sense bends. The results show that the folding deformations of such structure in the two cases are completely different. The equal-sense bending leads to the structure buckled abruptly, but gradual torsion buckling is received in the case of opposite-sense bending. The critical bending moments have big difference in the two cases, and the structure response is strongly dependant on the geometric parameters. Secondly, the critical buckling solution under pure bending was derived, and the result confirms to be agreeable with the finite element calculation.

Keywords: Shape memory polymer; Tape spring; Buckling analysis; Finite element

1 Introduction

The traditional metallic tape spring, also known as carpenter tape, has been extensively researched and applied in deployable space structures due to the advantages of low cost, low mass, self-locking function, stowage in a compact volume, deployment in large surfaces and/or large volumes, and others[1−4*etal*]. However, such structure requires a motor to provide power and damping mechanisms to ensure reliable and stable deploying. Thus it is complicated in design.

As considering the capability of self-frozen/deployment of thermal-activated shape memory polymers (SMPs) through a special thermomechanical cycle, new design concept and prototypes have been developed in deployable space structures by using continuous fiber-reinforced SMPs-based composites[5−9*etal*]. However, the ir-

[1] Department of Mechanics, School of Civil Engineering, Beijing Jiao-Tong University, Beijing, 100044, China

regular distribution of fibers in SMP matrix commonly causes pre-mature failure due to the local stress concentration.

This paper aims to investigate a new type of composite tape springs, which is consisted of one layer of metal and one layer of SMP. The advantage of such composite tape spring is that the metallic layer can present a high stiffness while SMP-layer has the function of shape frozen/recovery. Numerical simulation and theoretical analysis will be carried out on the non-linear responses (critical buckling and post-buckling) of such structure under bending. Further work will focus on their shape frozen/recovery behaviors.

2 Numerical simulation of metal/SMP tape spring under bending

2-D behaviors of the metal/SMP tape spring were numerically researched for two types of folds: equal-sense and opposite sense as seen in Fig. 1. ABAQUS commercial software was used and S4R5 shell element was selected. Fig. 2 presents the geometrical schematic of the metal/SMP tape spring in this study, which consists of an outer layer of metal and an inner layer of SMP (z_m=0.1 mm and z_e=5 mm). The material's parameters are listed in Table. 1.

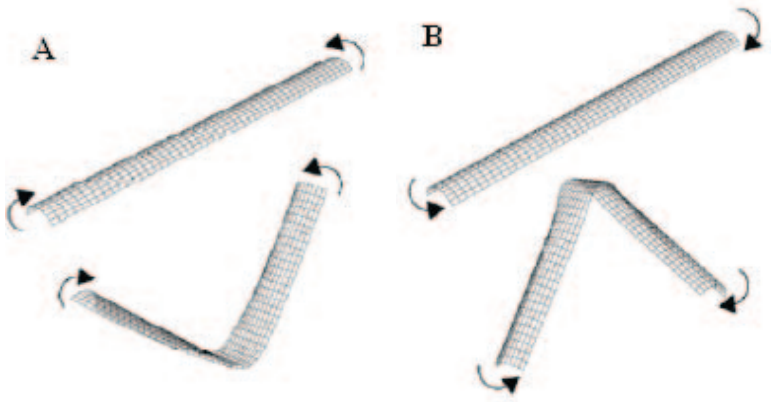

Figure 1: Folding of a tape spring: (A) opposite-sense bending (B) equal-sense bending

Fig. 3 shows the distribution of Von-mises stress when the metal/SMP tape spring subjected to opposite-sense bending. Before loading, there is no deformation (Fig. 3A). When a small bending angle is applied, the significant tensile and compressive zones are developed (Fig. 3B). With further increasing the bending angle, an ellipse stress-concentration zone is developed in the middle of the specimen

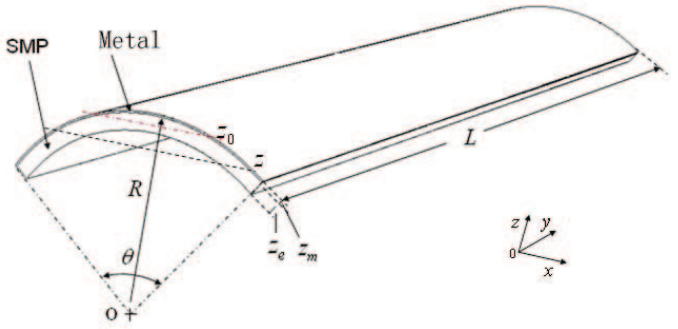

Figure 2: Schematic of a metal/SMP tape spring

Table 1: Material parameters

Parameter	Unit	Value	Description
E_e	Pa	5.74×10^6	Young's modulus of SMP-layer
E_{steel}	Pa	210×10^9	Young's modulus of Metal-layer
ν_{SMP}	–	0.4	Possion ratio of SMP-layer
ν_{steel}	–	0.3	Possion ratio of Metal-layer

(Fig. 3C). Then continuing increasing the bending angle, the shape of the stress-concentration zone develops from ellipse to rectangle and the stress in the two ends decreases significantly, which indicates that the structure is buckled (Fig. 3D). After buckling, the area of the stress concentration is increased with the bending angle (Figs. 3E and F). Similar deformation process is received when changing the geometer parameters (L, θ and R). So it means that the result is independent of the geometer parameters.

Fig. 4 shows the Von-mises stress distribution of a short-length metal/SMP tape spring (L=200 mm) subjected to equal-sense bending. Significant tensile and compressive zones are developed under the small bending angle (Fig. 4a). With increasing the bending angle, the stress concentration zone develops in the two edges of the middle zone (Fig. 4b). As further increasing the bending angle, the curvature radius in the stress concentration zone is significantly enlarged, which indicates that the structure is buckled (Figs. 4c and d). After that, the buckling zone is increased but its curvature radius keeps a nearly constant value (Figs. 4e and f). However, with increase of the length of the tape spring, the buckling is different (see Fig. 5). The critical buckling is happened in the two ends of the structure and companied with torsional deformation (Figs. 5c and d). With increase of the bending angle,

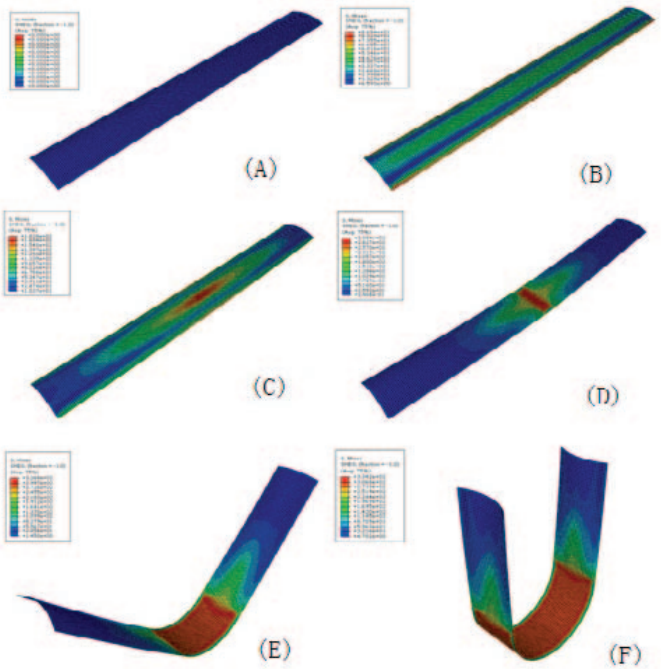

Figure 3: Stress distribution of tape spring under opposite sense bending: L=500 mm, R=50 mm, θ=60°

the buckling concentrates in the middle of the structure. The following deformation is similar with results in Fig. 4.

Table 2 list the critical buckling moments for metal/SMP tape spring with different lengths. It is clear that the length of the tape spring has significant influence on the critical buckling moment. Larger moments are required for the buckling of the structure at small length, which is due to the constraint at the two ends. When the length of the tape spring is larger than 600 mm, such influence becomes weak. The results also show a significant difference of the critical moments when the structure is under equal-sense and opposite-sense loads. When the structure is under opposite-sense load, the critical buckling is located in the middle of the structure and influences each other. Since it is close to the neutral center, the stress is small. When the structure is under equal-sense load, the critical buckling is located in the two edges of the structure and the constraint is weak. Hence the stress is large and the strcuture is easy to be buckled.

Table 3 presents the influence of the warp angle on the critical moments. The result confirms that the warp angle has a significant influence on the critical buckling

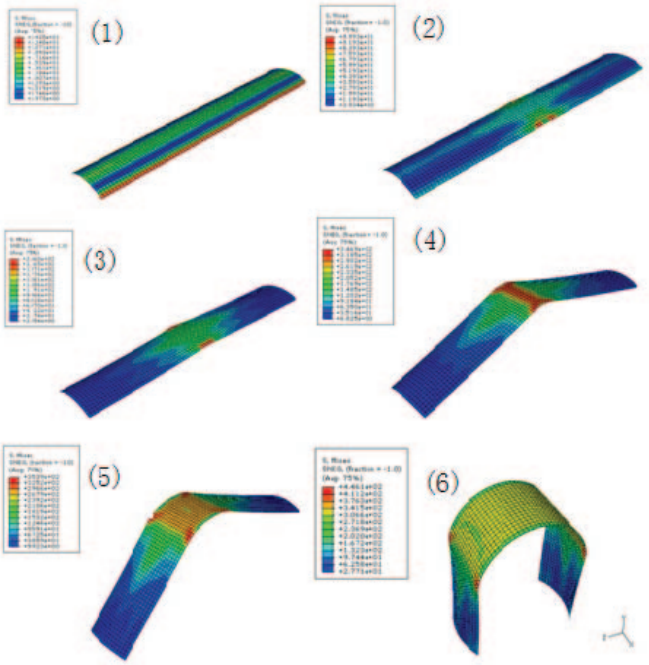

Figure 4: Stress distribution of a tape spring under equal-sense bending: L=200 mm, R=50 mm, θ=60°

Table 2: Length effect on the buckling moment: R=50mm, θ=60°

Angle (°)	300	400	500	600	700	800	1000
Opposite-sense moment (N·mm)	571	484	446	425	415	414	406
equal-sense moment (N·mm)	219	202	180	171	169	165	160

moments. Comparatively speaking, the warp angle has more strong influence when the structure is under opposite-sense load than that under equal-sense load. So we can change the critical buckling moments by changing the warp angle in design.

3 Theoretical solution of metal/SMP tape spring under bending

Fig. 6 presents the whole non-linear behaviors of a metal/SMP tape spring under equal-sense and opposite-sense bends. Linear relation between moment M and angle Θ exists before the critical buckling (E-O-A). After critical buckling (points A and E), M decreases significantly. A large local fold is created in the middle zone of the structure in the case of opposite-sense bending. But a flexural–torsional-mixed

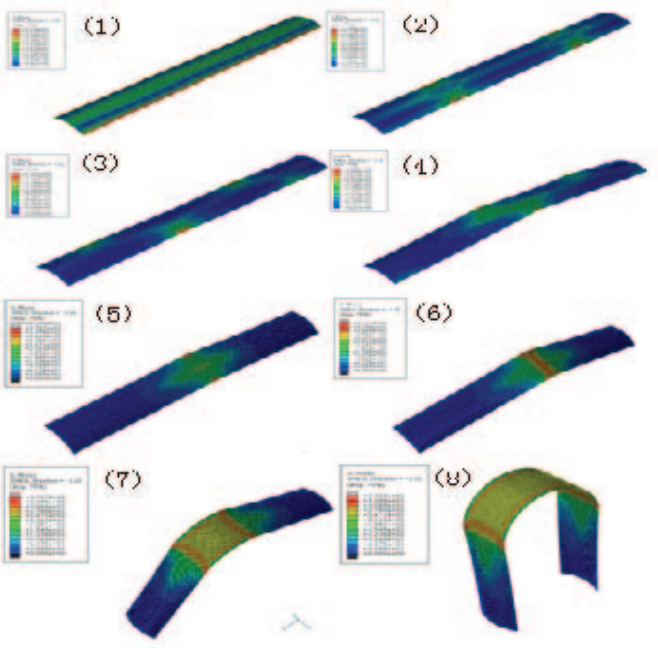

Figure 5: Stress distribution of a tape spring under equal-sense bending:L=500 mm, R=50 mm, θ=60˚

Table 3: Angle effect on the buckling moment: L=700 mm, R=50 mm (R=52.33 mm)

Angle (˚)	30	50	70	90	110	120
Opposite-sense moment (N·mm)	50 (105)	233 (300)	682(566)	1826(948)	4748 (1430)	7300 (1720)
equal-sense moment (N·mm)	12 (54)	94 (136)	295(217)	601	1038 (566)	1306 (660)

mode is observed in the case of equal-sense bending. With further increase of the rotation angle, the equal-sense and opposite-sense bending moments are respectively close to a constant value (B-C and F-G). Then curvature radius keeps nearly constant value, but the buckling length is increased.

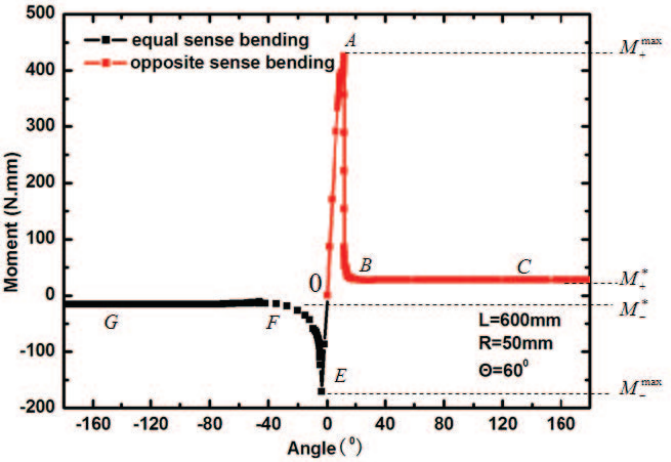

Figure 6: Bending moments of a metal/SMP tape spring

If we use a homogeneous material instead of such composite tape string, then the equal thickness is

$$H = \frac{E_m z_m^2 - 2 z_m z_e E_e - E_e z_e^2}{z_m E_m - z_e E_e} \tag{1}$$

When the strip is deformed from point A to point B (fFig. 6), the moment decreases abruptly, but the rotation has no significant change. During this process, the whole deformation energy U_A and the local deformation energy U_B are nearly equal:

$$U_A \approx U_B \tag{2}$$

The critical buckling deformation energy U_A can be expressed as

$$U_A = \frac{1}{2}\int_v \sigma \varepsilon_y dv = \frac{E_m}{2}\int_v \varepsilon_y^2 dv \tag{3}$$

where ε_y denotes the tension/compression strain along the Y-axis.

If we assume the critical buckling curvature radius to be ρ_{cr}, then the strain apart along the thickness of the specimen is

$$\varepsilon_y = \frac{z - z_0}{\rho_{cr}} \tag{4}$$

where z_0 denotes the distance of the neutral center apart from the coordinate axis. On condition of the pure bend, following relation exists along the cross section

$$\int_a \sigma da = 0 \tag{5}$$

where a denotes the area of the cross section. Thus

$$z_0 = \frac{R\sin(\theta/2)}{\theta/2} \tag{6}$$

Substituting Eqs. (4) and (6) into Eq. (3) receives

$$U_A = \frac{HLE_mR^3}{2\rho_{cr}^2}[\frac{\sin\theta}{4} - \frac{\sin^2\theta/2}{\theta/2} + \frac{\theta/2}{2}] \tag{7}$$

After buckling, assuming the curvature to be the function of buckling distance y and angle θ, thus

$$U_B = \frac{1}{2}\int_v E_m z^2 \psi(y,\theta)^2 dv = \frac{R\theta E_m H^3}{24}\int_0^{L/2} \psi^2(y,\theta)dy \tag{8}$$

Further assuming $\int_0^{L/2}\psi^2(y,\theta)dy = A_0 + A_1 e^{(A_2+A_3L)\theta}$, where A_0, A_1, A_2, A_3 are fitting constants, then Eq. (8) can be expressed as

$$U_B = \frac{R\theta E_m H^3}{24}[A_0 + A_1 e^{(A_2+A_3L)\theta}] \tag{9}$$

Substituting Eqs. (7) and (9) into Eq. (2) receives the critical buckling curvature radius as

$$\frac{1}{\rho_{cr}} = \frac{H}{2R}\sqrt{\frac{\theta(A_0 + A_1 e^{(A_2+A_3L)\theta})}{3L(\frac{\sin\theta}{4} - \frac{\sin^2\theta/2}{\theta/2} + \frac{\theta/2}{2})}} \tag{10}$$

Thus, the critical buckling moment under opposite-sense bending is

$$M_{cr}^+ = 2\int_0^{\theta/2}\sigma(z-z_0)da = 2\int_0^{\theta/2} E_m\varepsilon_y(z-z_0)da \tag{11}$$

Substituting Eqs. (4) and (6) into Eq. (12) receives

$$M_{cr}^+ = \frac{2HE_mR^3}{\rho_{cr}}(\frac{\sin\theta}{4} - \frac{\sin^2(\theta/2)}{\theta/2} + \frac{\theta}{4}) \tag{12}$$

According to the above FE calculating results listed in Tables 2 and 3, linear relation exists between the moments of equal-sense and opposite-sense bending. The factor is dependant on the arc length of the specimen. Thus following relation is assumed

$$M_{cr}^+ = \delta M_{cr}^- = [B_0 + B_1(S-B_2)^3]M_{cr}^- \tag{13}$$

By substituting the parameters of Table 1 into Eq. (13) and (14), the theoretical critical buckling moment are calculated. The fitting constants are listed in Table 4. Figs. 7 and 8 show the theoretical results and FE calculating values. It is clear that both are much agreeable.

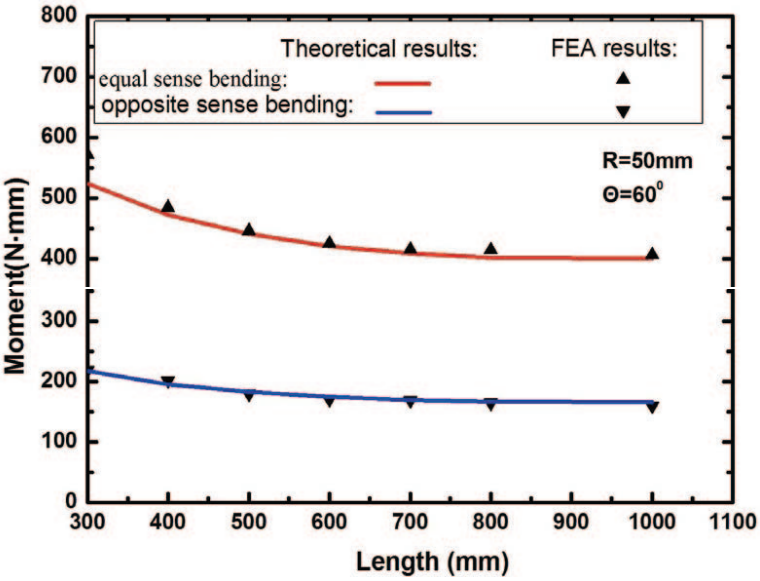

Figure 7: Relations between the length and critical moment

Table 4: Predictions of material constants

Constants	$A_0 \times 10^{-3}$	$A_1 \times 10^{-3}$	A_2	$A_3 \times 10^{-3}$	B_0	$B_1 \times 10^{-6}$	B_2
Values	4.9	1.3	0.92	1.4168	2.22	5.6	22

4 Conclusions

FE simulation was carried out on the non-linear bending behaviors of metal/SMP tape spring under equal-sense and opposite-sense bends. The results confirm that the bending behaviors in the two cases are much different: abrupt buckling in the case of opposite-sense bending and flexural–torsional-mixed mode in the case of equal-sense bending. Moreover, theoretical solutions of the critical buckling in the two cases are derived, which is much agreeable with the FE results.

Acknowledgement: This work was funded by Natural Science Foundations of China (No 11072027, 10872025), the Fundamental Research Funds for the Central Universities and Ministry of Education of the People's Republic of China (NECT).

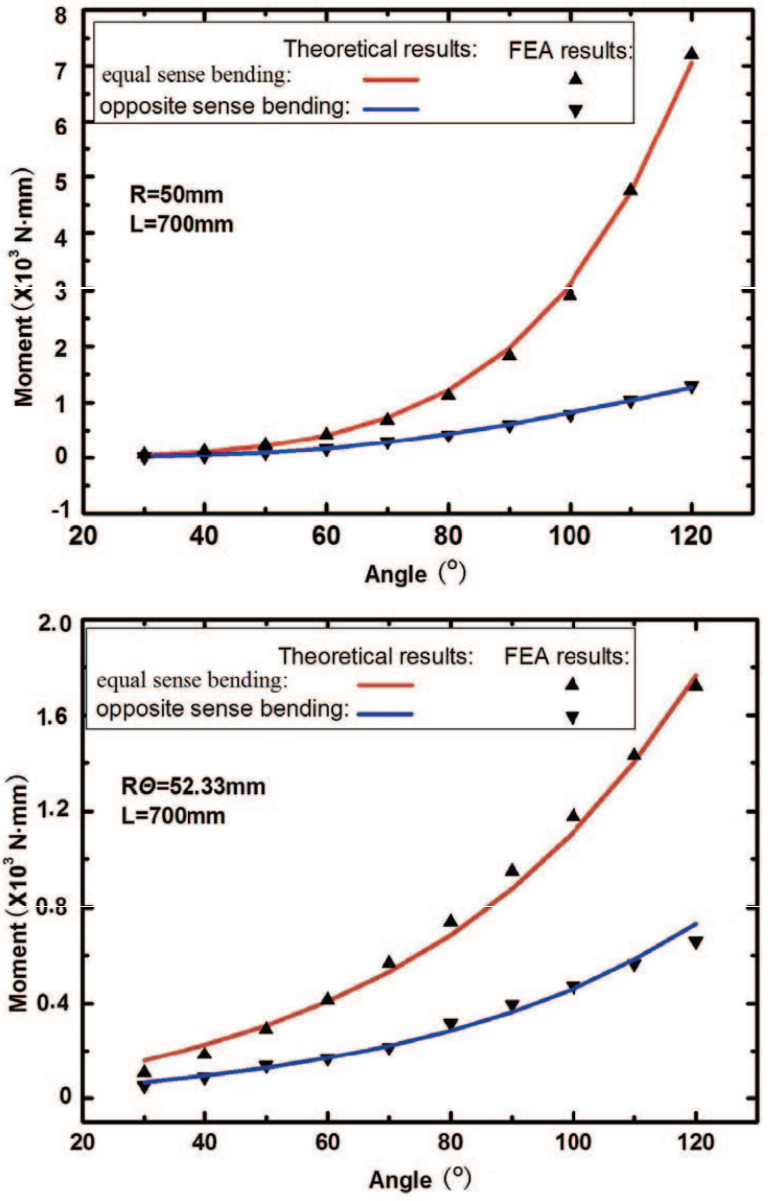

Figure 8: Relations between the angle and critical moment

References

[1] Wuest W. Einige anwendungen der theorie der zylinderschale. Zeitschrift fur angewandte Mathematik und Mechanik 1954; 34:444–54.

[2] Mansfield EH. Large-deflection torsion and flexure of initially curved strips. Proceedings of the Royal Society London 1973; A334:279–98.

[3] Seffen KA, Pellegrino S. Deployment dynamics of tape springs. Proceedings of the Royal Society of London 1999; A455:1003–48.

[4] Black J T, Whetzal J A, Blonk B J. Massarello J J. Deployment repeatability testing of composite tape springs for space optics applications. AIAA Journal, 2006, AIAA Paper No. 2006-1905.

[5] Black J T, Whetzal J A, Blonk B J. Massarello J J. Deployment repeatability testing of composite tape springs for space optics applications. AIAA Journal, 2006, AIAA Paper No. 2006-1905.

[6] Campbell D, Barrett R, Lake M S, et al. Development of a novel, passively deployed solar array [J]. AIAA Journal, 2006, AIAA Paper No. 2006-2080.

[7] Hazelton C S, Gall K R, Abrahamson E R, et al. Development of a prototype elastic memory composite STEM for large space structures. AIAA Journal, 2003, AIAA 2003-1977.

[8] Steven C A, Michael L T, Mark S L, Rory B. Elastic memory composites (EMC) for deployable industrial and commercial applications. Industrial and Commercial Applications of Smart Structures Technologies, San Diego, CA, USA, 2005.